NeuroImage **15,** 159–166 (2002)
doi:10.1006/nimg.2001.0962, available online at http://www.idealibrary.com on IDEAL®

The Influence of Brain Tissue Anisotropy on Human EEG and MEG

J. Haueisen,* D. S. Tuch,† C. Ramon,‡ P. H. Schimpf,§ V. J. Wedeen,† J. S. George¶ and J. W. Belliveau†

**Biomagnetisches Zentrum, Friedrich-Schiller-Universität, Jena, Germany; †Massachusetts General Hospital NMR Center, Charlestown, Massachusetts; ‡Department of Electrical Engineering, University of Washington, Seattle, Washington; §School of Electrical Engineering and Computer Science, Washington State University, Spokane, Washington; and ¶Los Alamos National Lab, Biophysics Group, Los Alamos, New Mexico*

Received April 7, 2000

The influence of gray and white matter tissue anisotropy on the human electroencephalogram (EEG) and magnetoencephalogram (MEG) was examined with a high resolution finite element model of the head of an adult male subject. The conductivity tensor data for gray and white matter were estimated from magnetic resonance diffusion tensor imaging. Simulations were carried out with single dipoles or small extended sources in the cortical gray matter. The inclusion of anisotropic volume conduction in the brain was found to have a minor influence on the topology of EEG and MEG (and hence source localization). We found a major influence on the amplitude of EEG and MEG (and hence source strength estimation) due to the change in conductivity and the inclusion of anisotropy. We expect that inclusion of tissue anisotropy information will improve source estimation procedures.

INTRODUCTION

The electrical conductivity of brain tissue, particularly white matter, is known to be anisotropic (Geddes *et al.,* 1967; Nicholson, 1965; Okada *et al.,* 1994; Polk *et al.,* 1986; Ranck, 1963; van Harreveld *et al.,* 1963). However, current modeling approaches applied to source localization based on EEG and MEG data neglect anisotropic electrical conductivity in the brain. Therefore, this simulation study was designed to assess the influence of anisotropy on both EEG and MEG.

For this purpose, we applied the high resolution finite element method (FEM) modeling of the human head that we have used in the past (Haueisen *et al.,* 1995, 1997; Schimpf *et al.,* 1998). Two major problems are connected with high resolution FEM modeling: (i) accurate tissue segmentation is both difficult and time consuming and (ii) the conductivity values needed are not reliable. Both problems can be overcome through the new technique of diffusion tensor magnetic resonance imaging from which individual conductivity tensor information can be derived for every patient (Tuch *et al.,* 1998, 1999). The technique does not measure the conductivity tensor directly but rather infers the conductivity tensor from the diffusion tensor based on a model of the two transport processes. The model predicts a strong linear relationship between the conductivity and diffusion tensors due to the fact that the transport for both processes is mediated principally through the extracellular space (Tuch *et al.,* 1999). The conductivity tensor map derived from the diffusion tensor image provides anisotropic conductivity values for each voxel. Thus, using the conductivity tensor maps it is possible to quantify the influence of anisotropy in the brain on the electric surface potential and the magnetic field.

We quantified this influence by comparing simulated EEG and MEG maps using three different types of volume conductor models: (i) a detailed inhomogeneous model with anisotropic conductivity tensors, (ii) a detailed inhomogeneous model with isotropic conductivity values, and (iii) a three-compartment model with isotropic conductivity values. The three-compartment model with isotropic conductivity values is additionally included because it is most widely used in source localizations based on EEG and MEG data.

MATERIALS AND METHODS

Measurements

A T1-weighted and a diffusion weighted tensor MRI scan of a healthy volunteer were obtained in one recording session (1.5 T GE Signa, General Electric, U.S.A.). The T1 scan consisted of a SPGR gradient echo with TR/TE = 24/8 ms and 102 slices with a thickness of 1.6 mm and a pixel size of 1×1 mm^2. The diffusion tensor scan employed a balanced pulsed-gradient spin echo (Reese *et al.,* 1998) with TR/TE/τ = 3000/93/30 ms, $b = 577$ s/mm^2, 8 averages with $1.56 \times 1.56 \times 3.2$ mm^3 voxels. The six diffusion gradients ($g = 14.14$ mT/m) were directed toward the nonopposed edges of a cube in *k*-space, and one null image was acquired in order to normalize for nondiffusion attenuation. Data were re-

1053-8119/02 $35.00

corded at the Massachusetts General Hospital (NMR Center, Charlestown, MA). The conductivity tensor was derived from the diffusion tensor (see next section) through the use of an empirical scaling of 0.736 S · s/mm^3 (Siemens · seconds/millimeter^3) as inferred from reported conductivity measurements (Tuch *et al.*, 1998, 1999).

Conductivity Tensor

The conductivity tensor σ describes the directional dependency of the conductivity, also known as anisotropy. Generally, σ is an asymmetric second-rank tensor (3×3 matrix in the three-dimensional case). Ohm's law describes the coupling between the current density vector $\vec{J}$ and the electrical field $\vec{E}$ through σ:

$$\hat{J} = \sigma\hat{E}. \quad (1)$$

It can be shown that for curl $\vec{E} = 0$ the conductivity tensor σ can be reduced to a symmetric tensor ($\sigma_{ik} = \sigma_{ki}$). Further, each symmetric second-rank tensor can be transformed to a diagonal form by choosing adequate coordinate axes ($\sigma_{ik} = 0$ for $i \neq k$) (Danielson, 1997).

The lack of a technique for robust measurement of the electrical conductivity tensor *in vivo* has discouraged the inclusion of anisotropic conductivity information in the electromagnetic source imaging forward model. Recently, however, investigators have proposed a model for inferring the electrical conductivity tensor from the water self-diffusion tensor measured by diffusion tensor magnetic resonance imaging (Basser *et al.*, 1994; Tuch *et al.*, 1998). The model is based on the premise that while conductivity and diffusion are mediated by different carriers, respectively cellular ions and water, both processes are functions of the underlying tissue microgeometry. If the two tensors are assumed to share eigenvectors based on the common geometry, then the model needs only to explain the scaling relationship between the tensor eigenvalues. In the quasi-static regime the intracellular conductivity is effectively shielded by the high impedance of the cell membrane. Hence, in the limit of small apparent intracellular diffusion both conductivity and diffusion are mediated principally by extracellular pathways. The eigenvalues are then linearly related and the tensors are related by $\sigma = \sigma_e/d_e D$, where σ_e and d_e are respectively the effective extracellular conductivity and diffusivity, and D is the diffusion tensor. The linear relationship can be derived more formally with a self-consistent effective medium model (Sen *et al.*, 1989; Tuch *et al.*, 1999) or a matrix formalism (Tuch, unpublished data). The scaling factor can be approximated from values for the extracellular transport coefficients or from comparison of conductivity and diffusion measurements. The linear approximation to the full effective medium relation was employed in the present study.

Figures 1a and 1b show an example of a T1-weighted MRI slice and the diffusion tensor.

The coordinate system used throughout the paper is indicated in Fig. 1d, where the x coordinate is from anterior to posterior, the y coordinate from superior to inferior, the z coordinate from left to right. The origin is at the first (left) slice at the anterior and superior corner.

Model Construction

Eleven different tissue types were segmented from the T1-weighted MR scan (Haueisen *et al.*, 1995) (Fig. 1c). Based on these segmentation results three different types of volume conductor models were constructed:

- Model I includes anisotropic conductivity tensor values for gray and white matter and isotropic conductivities for the other nine tissue types.
- Model II comprises isotropic conductivity values for all eleven tissue types.
- Model III consists of three compartments with isotropic conductivity values.

Table 1 gives the resistivity values used in the three models. The isotropic resistivity values were obtained from the literature as described in Haueisen *et al.* (1995). The anisotropic conductivity values for model I were voxel based. Thus, we give here only an example of an average of 27 voxels of gray matter surrounding the position of dipole 1 (see below) and of an average of 27 voxels of white matter anterior to the position of dipole 7. For gray matter we obtained $\sigma_{xx} = 0.41 \pm 0.18$ S/m, $\sigma_{xy} = 0.016 \pm 0.016$ S/m, $\sigma_{xz} = 0.019 \pm 0.014$ S/m, $\sigma_{yy} = 0.47 \pm 0.24$ S/m, $\sigma_{yz} = 0.016 \pm 0.011$ S/m, $\sigma_{zz} = 0.16 \pm 0.10$ S/m, and for white matter $\sigma_{xx} = 0.29 \pm 0.18$ S/m, $\sigma_{xy} = 0.019 \pm 0.013$ S/m, $\sigma_{xz} = 0.032 \pm 0.022$ S/m, $\sigma_{yy} = 0.61 \pm 0.28$ S/m, $\sigma_{yz} = 0.058 \pm 0.037$ S/m, $\sigma_{zz} = 0.28 \pm 0.10$ S/m (mean $\pm$ standard deviation, coordinate system as indicated above). The resulting eigenvalues for gray matter are $\sigma_1 = 0.566 \pm 0.180$, $\sigma_2 = 0.340 \pm 0.148$, $\sigma_3 = 0.136 \pm 0.097$, and for white matter are $\sigma_1 = 0.664 \pm 0.228$, $\sigma_2 = 0.346 \pm 0.123$ and $\sigma_3 = 0.179 \pm 0.113$.

The finite element mesh for all three models was generated through the connection of all slices. In this way, a grid of 1,456,069 hexahedral elements (voxels) with a resolution of $1 \times 1 \times 3.2$ mm was established. Based on this grid, a linear system of equations was set up and solved iteratively by means of a preconditioned conjugate gradient method (Hageman *et al.*, 1981). For the sake of a smoother error distribution, 100 Successive Over-Relaxation (SOR) iterations (relaxation factor, ω, fixed to 1.0) were performed after the convergence of the conjugate gradient solver. The

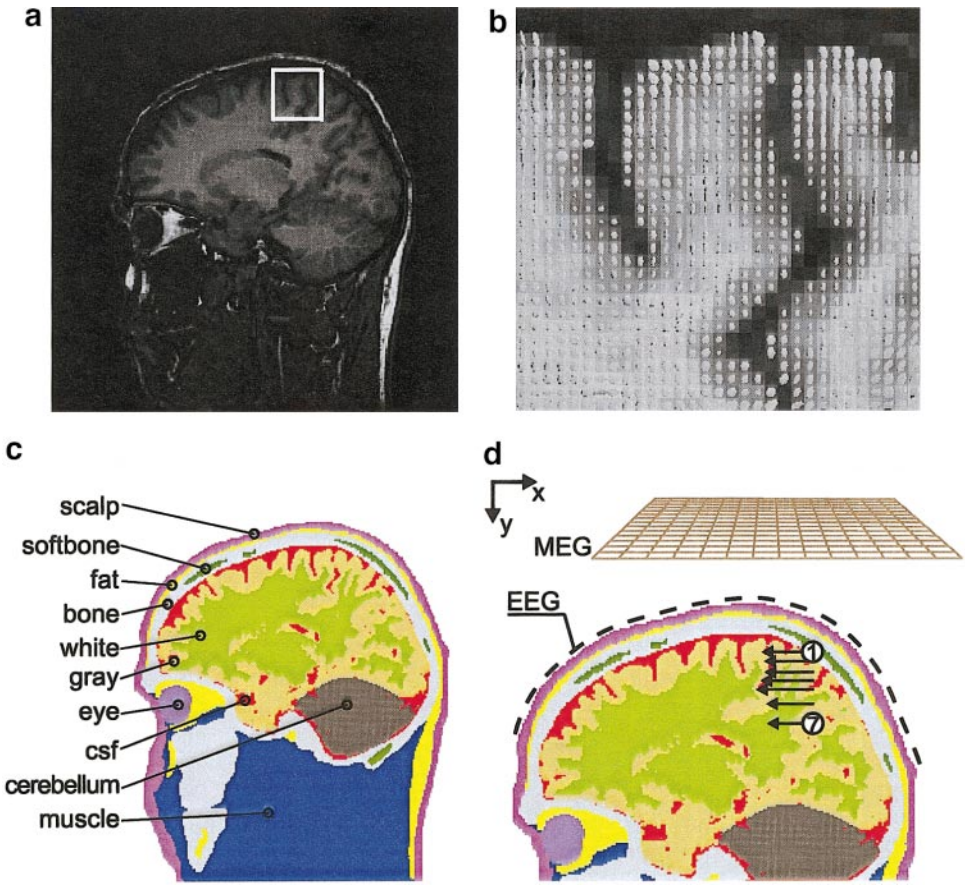

FIG. 1. Coregistered T1-weighted magnetic resonance image (a) and diffusion tensor (b), FEM model cross section (c), and setup for the simulations (d). The white square in (a) indicates the region of interest enlarged in (b). The diffusion tensor image was interpolated to match the spatial resolution of the T1 image. The ellipsoids depict the local diffusion tensor. The ellipsoid axes are oriented in the direction of the tensor eigenvectors and scaled according to the eigenvalues. The origin of the coordinate system is at the upper left corner of the first MR slice. The position of the dipoles 1 to 7 is indicated by the tip of the arrows (d). The dashed line in (d) illustrates the coverage of the electrodes only. The electric potential was actually computed at 300 single surface nodes of the FEM model.

convergence of the conjugate gradient solver was ensured by two criteria: first, the L2 norm of the system matrix of the linear system of equations had to drop so that the first five significant digits did not change anymore, and secondly, the potential difference had to decrease continuously during the iteration process.

For a given hexahedral element the current density J_e is defined in the center of the element by multiplying the element conductivity with the voltage gradient in the element. The components of this gradient are calculated by averaging the voltage of each side of the brick and computing the difference between two opposite sides. The magnetic field due to the current densities was computed using the Biot-Savart law. The source current term (current from sink to source) was included into the magnetic field computations by integrating the outward flow of each individual pole on a surface surrounding the pole and averaging the results of the two poles of each dipole.

TABLE 1

Human Tissue Types and Resistivity Values in Ωcm

	Model		
Tissue type	I	II	III
Brain white matter	CT	700	300
Brain gray matter	CT	300	300
Spinal cord and cerebellum	650	650	300
Cerebrospinal fluid	56	56	300
Hard bone	16,000	16,000	16,000
Soft bone	2,500	2,500	16,000
Muscle	1,000	1,000	300
Fat	2,500	2,500	300
Eye	200	200	300
Scalp	230	230	300
Soft tissue	500	500	300

Note. CT indicates that conductivity tensor information is used for each voxel of this tissue type.

Simulations

The goal of the simulations was to quantify the influence of anisotropy and inhomogeneous isotropic conductivity on the electric potential V and the magnetic field B. Thereto, we used both dipolar and extended sources positioned in models I through III. All sources were modeled by two fixed voltages at adjacent nodes.

Seven dipolar sources in different depths (20, 26, 32, 38, 45, 52, and 64 mm below the scalp, located in the motor cortex about 2.4 cm away from the longitudinal fissure of the cerebrum) were applied. All dipoles pointed into x direction and were thus roughly tangential to the scalp surface. Except for the deepest dipole, which was in the white matter, all positions were within the gray matter (Fig. 1d).

The extended sources were constructed by adding dipoles to an initial single dipole, which was located 32 mm below the scalp (number 3 of the 7 dipoles described above was shifted one node into left and one node into anterior direction). The first extended model consisted of 9 dipoles centered around the initial dipole within the anterior wall of the central sulcus. The spacing of the dipoles was 3 mm in y direction and 3.2 mm in z direction, and consequently the area covered was about 0.38 cm^2. The second extended model comprised 23 dipoles centered around the initial dipole with the same spacing and an area covered of about 1.5 cm^2. The third extended model was composed of 44 dipoles covering an area of approximately 3.1 cm^2. All dipoles pointed into x direction.

The electric surface potentials were taken from the node potentials on the surface of the scalp. The current density was calculated in the middle of each element from the adjacent node potentials. The magnetic field was computed in a sampling plane (15 $\times$ 15 grid, spacing of 1.0 $\times$ 1.0 cm) located at a distance of 2.3 cm above the head. The surface potentials were computed at 300 locations equally distributed on the scalp (common average reference; Fig. 1d).

Changes in the topography of fields or potentials are linked to changes in the dipole localization, while changes in the magnitude of fields or potentials are linked to changes in the source strength. In order to assess both changes, we computed the correlation coefficient (CC) and the deviation of magnitude (DM). CC and DM were calculated between the results based on models I (anisotropic) and II (isotropic), as well as between those based on models II (isotropic) and III (three compartments). We defined DM for magnetic fields (DMM) according to:

$$\mathrm{DMM} = \frac{\sum_{i=1}^{225} |B_i^{\mathrm{II}}| - \sum_{i=1}^{225} |B_i^{\mathrm{I}}|}{\sum_{i=1}^{225} |B_i^{\mathrm{II}}|} \cdot 100, \qquad (2)$$

where summation is over all sampling points i. B^{I} indicates the magnetic field computed with model I and B^{II} with model II. Analogously, we defined DMM between models II and III, where again model II serves as reference (denominator in Eq. (2)). DMM was computed separately for B_x, B_y, and B_z. Similarly, we defined the deviation of magnitude for electric potentials (DME).

RESULTS

We found a high correlation between the magnetic fields and electric potentials computed with the isotropic and the anisotropic model. The correlation coefficients for the B_y component in Fig. 2 (the component measured by common biomagnetometers) are above 0.99, except for the two deepest dipoles where they are above 0.98. The B_x component exhibits a lower correlation coefficient than the other two components of the magnetic field and the electric potential.

The deviation of magnitude is in general relatively high (average -31% for the single dipoles and -16% for the extended sources). The negative percentage values indicate that the magnitude computed with the anisotropic model is larger than the magnitude computed with the isotropic model (Eq. (2)). For the single dipoles in Fig. 2 there is a tendency of increasing V and B magnitude computed with the anisotropic model with increasing dipole depth.

The correlation between the magnetic fields and electric potentials computed with the isotropic model and the three-compartment model is high (Fig. 3). CC of the B_y component is above 0.99. CC of V is above 0.99 for the single dipoles but only above 0.97 for the extended sources. CC of the B_x component is again lower than CC of the other components.

The deviation of magnitude for single dipoles is in general smaller than in the comparison of the anisotropic and isotropic model above (average 8%), while the absolute values of DM for the extended sources are similar (average 16%). Here, the negative percentage values indicate that the magnitude computed with the three-compartment model is larger than the magnitude computed with the isotropic model (Eq. (2)). It is interesting to note the tendency that the magnetic field magnitude increases from model III to model II and again from model II to model I (negative values in Fig. 2 and positive values in 3), whereas this is not the case for the electric potential magnitude.

Figure 4 illustrates the correlation between isotropic and anisotropic volume currents in the sagittal slices of the FEM model. There are three distinct sections in the sequence of slices in Fig. 4. First, the outermost slices (1, 2, 50, and 51) show high correlation coefficients close to the correlation coefficients shown in Fig. 2. Second, around the position of the dipole singularities in the CC curves are observed. Third, in between the

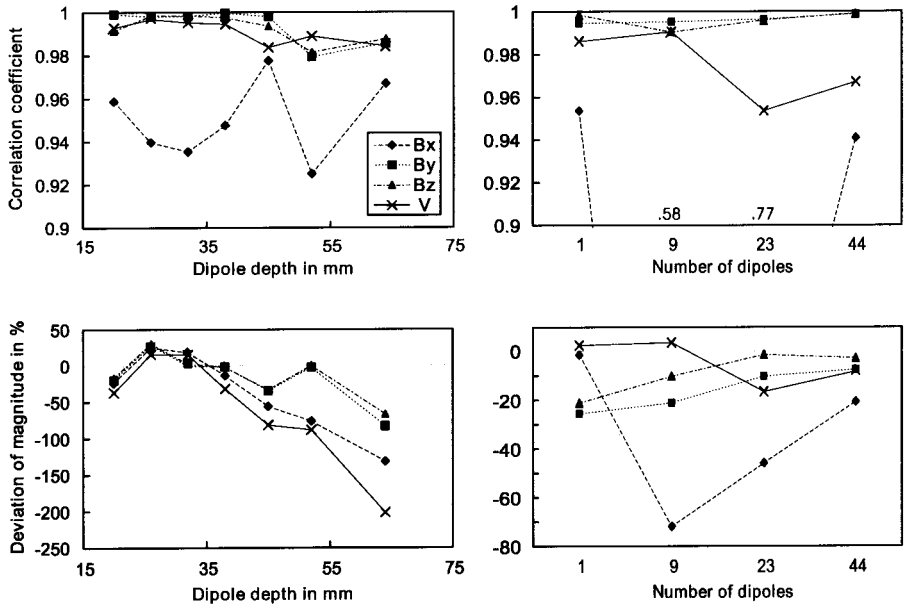

FIG. 2. Model I (anisotropic) versus model II (isotropic). Correlation coefficients (upper row) and magnitude changes (lower row) for single dipoles (left column) and extended sources (right column) for the magnetic field components B_x, B_y, B_z and the electric potential V. For comparability, the scales of the correlation coefficient axes are the same in all figures. The values cut are given as numbers.

dipole position and the outermost slices a clear depth dependance is present (the deeper the dipole the lower the volume current correlation).

Tables 2 and 3 give the comparison between models I through III for three dipoles at the position of dipole 1 in Fig. 1 pointing into x, y, and z direction. Since the dipole position is about 2.4 cm away from the longitudinal fissure of the cerebrum only the dipole pointing into x direction is a completely tangential dipole. The dipole pointing into z direction is mainly tangential with a small radial component, and the dipole pointing into y direction is mainly radial with a small tangential component.

For each dipole in Tables 2 and 3 CC reaches the lowest value for the magnetic field component into which the dipole is pointing. When comparing model I

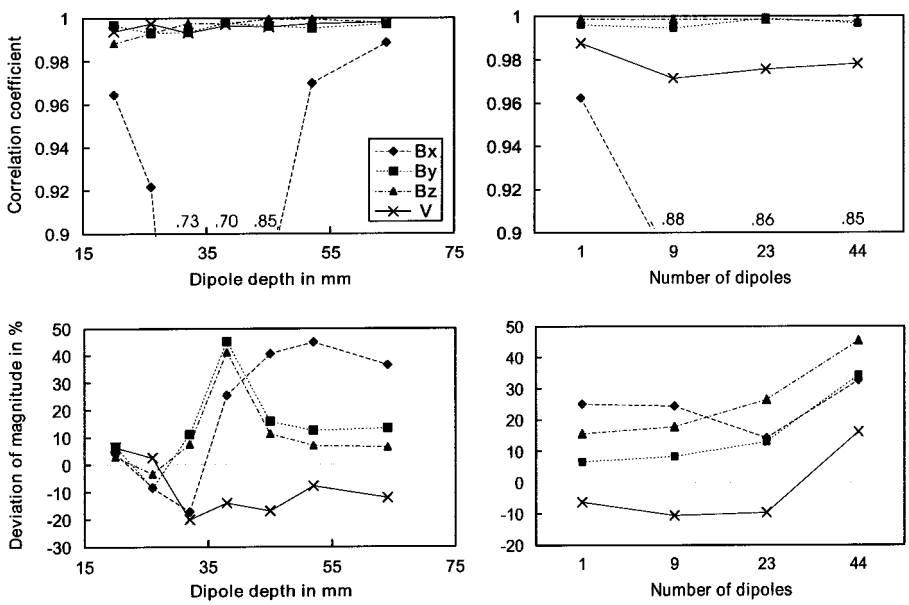

FIG. 3. Model II (isotropic) versus model III (three compartments). Correlation coefficients (upper row) and magnitude changes (lower row) for single dipoles (left column) and extended sources (right column) for the magnetic field components B_x, B_y, B_z and the electric potential V.

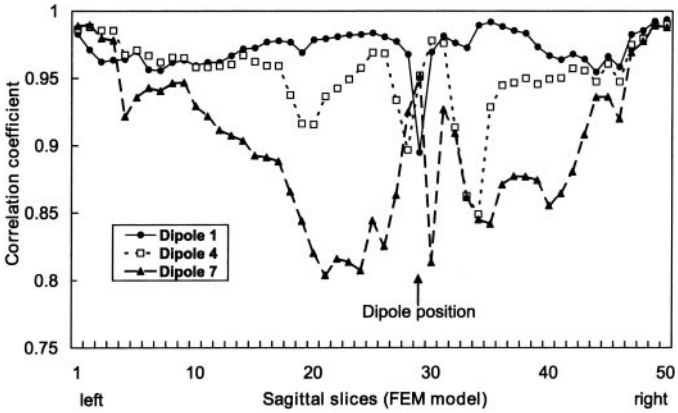

FIG. 4. Model I (anisotropic) versus model II (isotropic). Correlation coefficients for the volume currents (absolute magnitude) in all sagittal slices of the FEM model. Dipole 1 is the most superficial and dipole 7 the deepest dipole. Dipole 7 is within white matter.

with model II (Table 2), the lowest correlations were found for the more radially oriented dipole (*y* direction). However, when comparing models II and III, the dipole pointing into *z* direction exhibits the lowest values of CC.

DISCUSSION

According to our experiences in the analysis of modeling errors, a correlation coefficient of 0.98 could produce a dipolar source localization error of about 5–8 mm (in worst cases up to 1.5 cm) while a correlation coefficient above 0.99 will result in a localization error of approximately 1 mm at the most (Haueisen *et al.*, 1999; Jazbinsek *et al.*, 1999). Thus, for the single dipoles or small extended sources in the cortical gray matter investigated, the influence of anisotropy on MEG/EEG source localization is mostly within the principal accuracy of the common localization procedures. The amplitude changes observed translate with approximately the same percentage value into source strength changes. Since also the conductivity values changed between the isotropic and anisotropic model, we cannot attribute the amplitude changes directly to the inclusion of anisotropy. Nevertheless, we expect that MEG/EEG source strength estimation will improve when tissue anisotropy and individual tissue conductivity values are considered.

TABLE 2

Model I (Anisotropic) versus Model II (Isotropic)

	Dipole orientation	B_x	B_y	B_z	V
	x	0.940	0.998	0.998	0.997
CC	y	0.997	0.905	0.998	0.895
	z	0.989	0.995	0.985	0.945
	x	25.1	28.7	30.4	15.6
DM	y	7.9	44.7	8.4	−24.9
	z	17.7	6.6	−9.5	13.4

Note. Correlation coefficients (CC) and magnitude changes (DM) for dipoles pointing into *x*, *y*, and *z* direction (dipole position fixed).

TABLE 3

Model II (Isotropic) versus Model III (Three Compartments)

	Dipole orientation	B_x	B_y	B_z	V
	x	0.922	0.993	0.993	0.997
CC	y	0.998	0.966	1.000	0.981
	z	0.994	0.970	0.815	0.952
	x	−8.3	−8.2	−3.3	2.7
DM	y	5.7	5.1	6.3	−116.1
	z	16.0	12.0	23.6	−15.9

Previously, we investigated the influence of tissue conductivity changes on the magnetic field and the electric surface potential and found that an accurate modeling of magnetic field and electric potential strength requires accurate knowledge of tissue conductivities, while this knowledge might not be a necessity for source localization procedures (Haueisen *et al.*, 1997, 2000). Similarly, in this paper tissue anisotropy and conductivity changes have a stronger influence on source strength estimation than on source localization. Moreover, an analogous influence was found when comparing an isotropic three-compartment model (model III) with a detailed isotropic model (model II). A paper by Cuffin (1991) demonstrated a similar effect (small influence on the MEG/EEG topology but significant influence on amplitudes) with conductivity changes in a small eccentric sphere (bubble) within a three-layer concentric spherical model. Further, anisotropy in the innermost layer of a four layer spherical volume conductor had a strong effect on the magnitude of the electric potential produced by a tangential dipole, but only a weak effect on the topology (Zhou *et al.*, 1992). Given these lines of evidence, one might conclude that amplitudes are in general more sensitive to conductivity changes (including anisotropic conductivity) than topologies.

The component of the magnetic field that is aligned with the dipole orientation is more sensitive to model changes than the other two magnetic field components. This holds for extended and single dipolar sources (e.g., B_x in Fig. 2 or CC in Tables 2 and 3). However, the maxima of the magnitude of this component are on average only 35 ± 5% (mean ± standard deviation; for extended sources) of the other two magnetic field components. Thus, its magnitude is much smaller and is more sensitive to model changes. This behavior is expected due to the cross product term in the Biot-Savart law.

The depth dependance in Fig. 4 (the deeper the dipole the lower the volume current correlation between models I and II) can be explained by the larger amount of anisotropic tissue in the surrounding of the deeper dipoles. The different shapes of the singularities in the CC curves observed around the position of the dipole in Fig. 4 are most likely due to the different local conductivity profiles (the voxels very close to the dipole). Another conclusion from Fig. 4 is that the volume current topology inside the volume conductor might vary considerably, while the resulting magnetic field outside and the electric potential on the surface of the head exhibit a highly similar topology (Ramon *et al.*, 2000).

Voltage sources or current sources are used in EEG and MEG modeling. By a current source, one means a source with a specified current (or current dipole moment), i.e., the current does not depend on the load impedance (in this case, on tissue impedance). A voltage source produces a specified voltage, resulting in a current through the load impedance that is inversely proportional to impedance values. In this paper we have used a voltage source. The actual sources in the brain are neither pure voltage sources nor pure current sources. This means that both source current and the local electric field depend on local conductivity. Thus, for advanced source modeling information about the conductivities in the brain as provided by conductivity tensor imaging is of great importance.

The following limitations of the work presented are important. We considered only single dipolar or extended sources which are the most commonly used source models in MEG/EEG studies. The effect of multiple sources remains to be investigated.

Our results are based on isotropic tissue conductivities for the skull. The skull consists of three layers and it appears the inner layer has substantially higher conductivity. This implies that the conductivity of the full skull is larger in tangential directions than skull normal directions. Skull properties have a large effect on the EEG scalp distribution. Thus, we expect that the inclusion of skull anisotropy will further influence the electric potentials (Marin *et al.*, 1998; van den Broek *et al.*, 1998).

Although a general validation of the conductivity tensor imaging technique has been performed its error limits have not yet been completely investigated. They need to be quantified in future *in vivo* studies; e.g., voxel size is a crucial parameter. Fiber crossings within one voxel might yield substantially different conductivity tensor values for different voxel sizes or shifted voxels (e.g., the same voxel size in two scans of the same person in two sessions). The present study is based on data for one subject only. Although we do not expect changes in our main conclusions the values given in the result section might vary due to intersubject variability.

In conclusion, it seems that anisotropic volume conduction in the brain has a minor influence on MEG/EEG source localizations but might have a major influence on source strength estimations in the case of single dipoles or small extended sources in the cortical gray matter. Thus, inclusion of conductivity tensor information will improve source estimation procedures as well as imaging of potentials on the dura surface (Gevins *et al.*, 1999). Another advantage of the volume conductor modeling technique based on diffusion tensors MR is the decreased expenditure in the tissue segmentation of the brain. The improved sensitivity of the forward model due to the inclusion of the tissue anisotropy within source estimation algorithms (e.g., forcing dipoles out of the white matter or determining dipole orientation based on fiber geometry) will be evaluated in a future study. Moreover, this technique will be extended to ECG/MCG modeling where tissue anisotropy might be even more influential.

ACKNOWLEDGMENTS

This work was supported by a joint travel grant from the National Science Foundation (NSF, INT-9726712) and the German Academic Exchange Agency (DAAD). We thank the John von Neumann Institut for Computing, Jülich, Germany for providing the computer resources.

REFERENCES

Basser, P. J., Matiello, J., and Bihan, D. L. 1994. MR diffusion tensor spectroscopy and imaging. *Biophys. J.* **66:** 259–267.

Cuffin, B. N. 1991. Eccentric spheres models of the head. *IEEE Trans. Biomed. Eng.* **38:** 871–878.

Danielson, D. A. 1997. *Vectors and Tensors in Engineering and Physics.* Perseus Books, Reading, MA.

Geddes, L. A., and Baker, L. E. 1967. The specific resistance of biological materials—A compendium of data for the biomedical engineer and physiologist. *Med. Biol. Eng. Comput.* **5:** 271–293.

Gevins, A., Le, J., Leong, H., McEvoy, L. K., and Smith, M. E. 1999. Deblurring. *J. Clin. Neurophysiol.* **16:** 204–213.

Hageman, L. A., and Young, D. M. 1981. *Applied Iterative Methods.* Academic Press, New York.

Haueisen, J., Böttner, A., Nowak, H., Brauer, H., and Weiller, C. 1999. The influence of conductivity changes in boundary element compartments on the forward and inverse problem in electroencephalography and magnetoencephalography. *Biomed. Tech. (Berlin)* **44:** 150–157.

Haueisen, J., Ramon, C., Czapski, P., and Eiselt, M. 1995. On the influence of volume currents and extended sources on neuromagnetic fields: A simulation study. *Ann. Biomed. Eng.* **23:** 728–739.

Haueisen, J., Ramon, C., Eiselt, M., and Nowak, H. 1997. Influence of tissue resistivities on neuromagnetic fields and electric potentials studied with a finite element model of the head. *IEEE Trans. Biomed. Eng.* **44:** 727–735.

Haueisen, J., Ramon, C., Brauer, H., and Nowak, H. 2000. The influence of local tissue conductivity changes on the magnetoencephalogram and the electroencephalogram. *Biomed. Tech. (Berlin)* **45:** 211–214.

Jasbinsek, V., and Hren, R. 1999. Influence of randomly displaced BSPM leads on the identification of ventricular preexcitation cites. *Biomed. Tech. (Berlin)* **44**(Supp. 2): 104–107.

Marin, G., Guerin, C., Baillet, S., Garnero, L., and Meunier, G. 1998. Influence of skull anisotropy for the forward and inverse problem in EEG: Simulation studies using FEM on realistic head models. *Hum. Brain Mapp.* **6:** 250–269.

Nicholson, P. W. 1965. Specific impedance of cerebral white matter. *Exp. Neurol.* **13:** 386–401.

Okada, Y. C., Huang, J.-C., Rice, M. E., Tranchina, D., and Nicholson, C. 1994. Origin of the apparent tissue conductivity in the molecular and granular layers of the *in vitro* turtle cerebellum and the interpretation of Current Source-Density analysis. *J. Neurophysiol.* **72:** 742–753.

Polk, C., and Postow, E. (Eds.) 1986. *CRC Handbook of Biological Effects of Electromagnetic Fields.* CRC Press, Boca Raton, FL.

Ramon, C., Wang, Y., Haueisen, J., and Schimpf, P. 2000. Effect of myocardial anisotropy on the torso current flow patterns and magnetic fields. *Phys. Med. Biol.* **45:** 1141–1150.

Ranck, J. B. 1963. Specific impedance of rabbit cerebral cortex. *Exp. Neurol.* **7:** 144–152.

Reese, T. G., Weisskoff, R. M., and Wedeen, V. J. 1998. Diffusion NMR facilitated by a refocused eddy-current EPI pulse sequence. In *Proc. Sixth Ann. Meeting Int. Soc. Magn. Res. Med.,* p. 663. Sydney, Australia.

Schimpf, P., Haueisen, J., Ramon, C., and Nowak, H. 1998. Realistic computer modelling of electric and magnetic fields of human head and torso. *Parallel Comput.* **24:** 1433–1460.

Sen, A. K., and Torquato, S. 1989. Effective electrical conductivity of two-phase disordered anisotropic composite media. *Phys. Rev. B* **39:** 4504.

Tuch, D. S., Wedeen, V. J., Dale, A. M., and Belliveau, J. W. 1998. Electrical conductivity tensor map of the human brain using NMR diffusion imaging: An effective medium approach. In *Proc. Sixth Ann. Meeting Int. Soc. Magn. Res. Med.*, p. 572. Sydney, Australia.

Tuch, D. S., Wedeen, V. J., Dale, A. M., George, J. S., and Belliveau, J. W. 1999. Conductivity mapping of biological tissue using diffusion MRI. *Ann. NYAS* **888:** 314–316.

van den Broek, S. P., Reinders, F., Donderwinkel, M., and Peters, M. J. 1998. Volume conduction effects in EEG and MEG. *Electroencephalogr. Clin. Neurophysiol.* **106:** 522–534.

van Harreveld, A., Murphy, T., and Nobel, K. W. 1963. Specific impedance of rabbit's cortical tissue. *Am. J. Physiol.* **205:** 203–207.

Zhou, H., and van Oosterom, A. 1992. Computation of the potential distribution in a four layer anisotropic concentric spherical volume conductor. *IEEE Trans. Biomed. Eng.* **39:** 154–158.